Journal of Porous Materials
https://doi.org/10.1007/s10934-026-01925-y

Physicochemical characterization and in vitro evaluation of natural clinoptilolite zeolite on proliferation and migration of fibroblast and epithelial cell lines: Implications for periodontal wound healing

Nezahat Arzu Kayar[1] · Hasan Hüsnü Eren[2] · Bayram Ilkhan[3] · Ahmet Yilmaz Coban[3,4,5]

Received: 10 March 2026 / Accepted: 17 May 2026
© The Author(s) 2026

Abstract

This study aimed to characterize a natural clinoptilolite-type zeolite and evaluate its effects on proliferation and migration in L929 (fibroblast) and HEK293T (epithelial) cell lines. XRD analysis confirmed the material's high purity, with clinoptilolite as the dominant phase (72.9%). XRF and ICP-MS analyses demonstrated that the Si/Al ratio (4.8–5.4) and cation exchange capacity (CEC: 2.38 meq/g) were consistent with typical clinoptilolite. SEM revealed irregular, aggregated particles (7–10 µm) with high porosity. Cell proliferation (MTT assay) and migration (Scratch Wound Assay) were assessed. The zeolite showed a significant dose- and time-dependent proliferative effect on both cell lines. Notable increases in proliferation were observed at 500 µg/mL in L929 cells at 72 h ($p<0.0001$) and at 600 µg/mL in HEK293T cells ($p<0.0001$). Cell migration was also enhanced, particularly at 200 µg/mL in L929 ($p<0.01$) and 100 µg/mL in HEK293T ($p<0.001$). Overall, these results indicate that this high-purity clinoptilolite zeolite possesses the potential to support the proliferation and migration of key cell types involved in wound healing and thus holds great promise as a bioactive material for biomedical applications.

Keywords Zeolites · Clinoptilolite · Characterization · Cell proliferation · Cell movement · Regenerative dentistry

1 Introduction

The healing of periodontal tissues is a very dynamic and complicated biological process that includes the rearranging of epithelial cells, the activation of fibroblasts, the growth of new blood vessels, and the remodeling of the extracellular matrix (ECM) [1]. The efficacy of gingival wound healing is directly linked to both traditional surgical techniques and the performance of regenerative biomaterials. Many studies in the past few years have shown that biopharmaceutical agents like growth factors, enamel matrix derivatives, collagen-based membranes, and fibrin adhesives can help periodontal regeneration. Additionally, adjunctive technologies, including laser therapy and hyperbaric oxygen therapy, have shown potential to accelerate wound healing. However, the limited clinical applicability and high cost of these approaches have led to the search for alternative materials [1, 2]. Zeolites, which have a large surface area, can exchange ions, and are not very toxic, have been looked at as possible ways to help periodontal tissue grow back [2]. In the context of wound healing, zeolites have demonstrated

✉ Nezahat Arzu Kayar
narzu@hotmail.com

Hasan Hüsnü Eren
drhheren@gmail.com

Bayram Ilkhan
bayramilkhan@gmail.com

Ahmet Yilmaz Coban
aycoban@akdeniz.edu.tr

1 Faculty of Dentistry, Department of Periodontology, Akdeniz University, Antalya 07058, Türkiye

2 Private Office Dr. Eren, Nispetiye Mah. Nispetiye Cad., Özden İş Merkezi No:22, Istanbul, Turkey

3 Department of Medical Biotechnology, Akdeniz University, Institute of Health Sciences, Antalya, Turkey

4 Faculty of Health Sciences, Department of Nutrition and Dietetics, Akdeniz University, Antalya, Turkey

5 Faculty of Health Sciences Research Laboratory, Tuberculosis Research Unit, Antalya, Turkey

Published online: 06 June 2026

significant potential due to their hemostatic properties, ability to modulate the local ionic microenvironment through controlled cation release, and capacity to support cell adhesion via surface interactions. Recent studies have shown that zeolite-based materials can promote fibroblast proliferation, enhance epithelial cell migration, and accelerate tissue repair processes, making them promising candidates for regenerative applications in periodontal wound healing [3].

Natural zeolites are hydrated aluminosilicate minerals that have many uses in industry and the environment because they can exchange ions, adsorb, and act as catalysts. They make crystalline, lattice-like structures that have a lot of surface area and can choose which ions to bind to. Clinoptilolite, which is part of the Heulandite (HEU) structural family, is one of the most common and commercially important natural zeolites because it has a high silica-to-alumina ratio and is stable at high temperatures [3, 4]. Additionally, their unique structural properties allow for ion exchange, which means that natural zeolites can be functionalized with metal ions like silver (Ag^{+}), zinc (Zn^{2+}), copper (Cu^{2+}), calcium (Ca^{2+}), and strontium (Sr^{2+}) [2, 5].The tetrahedral framework of zeolites gives them a large internal surface area, and the fact that internal metal–oxygen tetrahedra can be chemically changed (for example, by exchanging cations, changing the Si/Al ratios, or adding metal particles) sets them apart from other crystalline inorganic oxides. They can also form a wide range of structures and compositions [6, 7]. Natural zeolites are known for having a high hydration capacity, a strong crystallinity, a low density, a large pore volume (after dehydration), shape selectivity, the ability to exchange ions, catalytic activity, the ability to adsorb molecules and ions, and a certain amount of electrical conductivity [7].

Zeolite also helps wounds and tissues heal because of the way its molecules are made, Ninan et al. created synthetic zeolites that were shown to improve the survival of NIH/3T3 fibroblasts and have antibacterial properties because they let more oxygen through. In an in vivo rat model, synthetic zeolites expedited the healing of skin ulcers within 20 days [8]. Neidrauer et al. produced a synthetic zeolite ointment that had nitric oxide in it. This ointment worked against a wide range of bacteria and sped up the healing of wounds without harming 3T3 fibroblasts. In vivo, NO–zeolite ointment improved wound closure more effectively than controls [9]. Mohandesnezhad et al. developed zeolite-infused nanofiber scaffolds that enhanced the proliferation of human dental pulp stem cells (hDPSCs) in vitro [10].

The available evidence suggests that both natural and synthetic zeolites demonstrate hemostatic activity and possess biological properties that facilitate cell proliferation and migration, underscoring their potential as novel agents for tissue regeneration. Their biocompatibility and non-cytotoxic characteristics across diverse cell types, coupled with numerous in vitro and in vivo studies illustrating their ability to expedite tissue repair, further substantiate their significance [9, 11, 12]. The L929 murine fibroblast cell line was chosen for the initial in vitro evaluation because it is a well-known standard for testing cytotoxicity and biocompatibility (ISO 10993–5). It provides a consistent way to measure basic fibroblastic responses that are important for gingival connective tissue. The HEK293T human embryonic kidney epithelial cell line was used to model the epithelial part of wound healing. HEK293T cells, although not sourced from oral mucosa, are a well-established and reliable model for investigating the fundamental mechanisms of human epithelial cell proliferation, migration, and signal transduction, owing to their high transfectability and consistent growth properties [13]. This well-known line makes it possible to do a controlled, high-throughput initial screening of zeolite's effects on epithelial behavior without the variability that is common with primary cells. Although HEK293T cells do not recapitulate the differentiated phenotype of oral keratinocytes, they serve as a well-validated and reproducible platform for the initial evaluation of biomaterial effects on fundamental epithelial cell behaviors, thereby minimizing inter-experimental variability and enabling standardized comparisons across studies [13]. This research signifies an essential initial phase; favorable outcomes derived from this model will require further confirmation in more physiologically pertinent oral epithelial cell cultures. While previous studies have primarily focused on synthetic or chemically modified zeolites, the present study uniquely investigates a natural, unmodified clinoptilolite-type zeolite through a comprehensive multi-technique physicochemical characterization (XRD, XRF, ICP-MS, SEM, BET, CEC) combined with systematic biological screening across two distinct cell types. This approach provides baseline data essential for the rational design of future functionalization strategies. Understanding how zeolites affect tissues that heal in complicated ways, like periodontal tissues, is an important step toward making better biomaterials. In this context, understanding how cells respond to zeolites represents a crucial first step toward their potential use in biomaterial research for oral tissues.. Although numerous studies have investigated chemically modified zeolites for wound healing, understanding the inherent biological activity of the unmodified natural material is a critical prerequisite for any rational functionalization strategy. Natural zeolites offer distinct advantages including cost-effectiveness, accessibility for large-scale applications, avoidance of complications associated with chemical modification (e.g., residual reagents and altered surface chemistry), and establishment of a baseline safety and efficacy profile essential for regulatory approval in biomedical applications. The current study involved a

thorough characterization of a high-purity clinoptilolite-containing natural zeolite utilizing XRD, XRF, ICP-MS, and SEM analyses. Additionally, a preliminary in vitro biological assessment was conducted to evaluate the cellular responses of fibroblast and epithelial cell lines subsequent to exposure to natural zeolite under regulated conditions.

2 Materials and methods

The mineralogical and chemical composition data of the natural zeolite were obtained from analyses performed at the Technology Application and Research Center (TUAM) laboratories of Afyon Kocatepe University.

2.1 Preparation of the zeolite sample

The natural zeolite used in this study (MORE THAN brand MHA–Micronized Heat Activated Clinoptilolite, CAS No: 12173–10-3) was obtained commercially. Before starting all characterization procedures, the sample was dried at 80 °C for 12 h to remove residual moisture and subsequently ground to a particle size of less than 100 µm toensure homogeneity for analysis. The < 100 µm specification refers to the sieve size used during the initial preparation stage to remove coarse particles and ensure a standardized upper particle size limit. The actual individual particle and aggregate dimensions, as observed by SEM (7–10 µm), are well within this sieved fraction and represent the true morphological characteristics of the prepared material.

2.2 X-ray diffraction (XRD) analysis

X-ray diffraction analysis was performed using a Bruker D8 Advance diffractometer equipped with Cu Kα radiation (λ = 1.5406 Å) to determine the crystal structure. Measurements were conducted in the Bragg–Brentano θ–2θ configuration under tube conditions of 40 kV and 30 mA. Scans were recorded over the 5–70° 2θ range with a step size of 0.02°. The obtained diffraction patterns were evaluated using the standard ICDD PDF database [14].

2.3 Scanning electron microscopy (SEM) analysis

Morphological characterization was carried out using a LEO 1430 VP scanning electron microscope. To make sure the surface was conductive, the powdered zeolite was put on carbon adhesive tape and covered with a thin layer of gold (Au) through sputtering. Imaging was performed using a secondary electron (SE) detector at an accelerating voltage of 20 kV and a working distance of 17 mm [15].

2.4 Chemical composition determination by XRF spectrometry

The major oxide components of the sample were determined using X-ray fluorescence (XRF) spectrometry. Prior to analysis, the sample was homogenized and prepared in accordance with the manufacturer's protocol. Quantitative evaluations were based on the measured oxide percentages [16].

2.5 Elemental analysis by ICP-MS

To measure trace elements, the sample was digested with the right acid mixture and then analyzed by ICP-MS. The manufacturer provided multi-element calibration standards that were used for measurement. Data processing followed standard methodologies that allow accurate quantification of low-level elemental concentrations.

2.6 BET surface area and pore structure analysis

The specific surface area and pore characteristics of the sample were determined from N_2 adsorption–desorption isotherms and calculated using the Brunauer–Emmett–Teller (BET) method. Prior to measurements, the sample was degassed under vacuum. The average pore diameter and bulk density were obtained using standard BET models [17].

2.7 Determination of cation exchange capacity (CEC)

The classical acetate exchange method, which uses NaOAc and NH_4OAc solutions, was used to find the cation exchange capacity. The sample was subjected to regulated pH and ionic strength conditions, and the ion exchange in the solution phase was measured. The CEC value was calculated using standard formulae [18].

2.8 Cell culture

In this study, the L929 (ATCC, CCL-1) fibroblast cell line and the HEK293T (ATCC, CRL-11268) epithelial cell line were used to simulate intraoral wound healing under in vitro conditions. L929 cells were cultured in RPMI-1640 medium supplemented with 10% fetal bovine serum (FBS), 1% non-essential amino acids, 1% sodium pyruvate, 0.5% L-glutamine, 0.5% gentamicin, and 0.02% amphotericin B. The cultured under the same conditions, using DMEM medium supplemented with the same additives. Once the cells reached approximately 70% confluence in culture

flasks, subculturing was performed, and the cells were prepared for experimental procedures.

The doses of natural zeolite to be evaluated were weighed, suspended in RPMI-1640 medium containing 1% FBS, and prepared for use in the experimental procedure.

2.9 MTT assay for cell viability

The MTT assay was used to see how zeolite affected the growth of L929 and HEK293T cells. Cells were placed in flat-bottomed 96-well plates at a density of 5×10^3 cells/200 µL per well and left to grow. After the cells had stuck to the well surface, the prepared zeolite doses (100–600 µg/ml) were added to the wells. In the initial study, a 90% reduction in cell viability was noted at doses of 1 mg/ml and higher, prompting the design of experimental concentrations accordingly. After 24, 48, and 72 h of incubation, 20 µL of MTT solution at a concentration of 5 mg/ml was added to each well and incubated for 4 h. After the incubation, the medium was taken out, and 100 µL of DMSO was put into each well to dissolve the formazan crystals that had formed. A microplate reader measured absorbance at 570 nm, and the data were analyzed using statistics. Cell viability was calculated using the following formula: Cell Viability (%) = (OD sample/OD control) × 100, where OD sample is the absorbance of treated cells and OD control is the absorbance of untreated control cells. Background absorbance (blank wells without cells) was subtracted from all readings before calculation. In the initial study, a 90% reduction in cell viability was noted at doses of 1 mg/mL and higher, prompting the selection of 100–600 µg/mL as the experimental concentration range. The Time Zero (T0) measurement represents the baseline cell viability reading taken immediately after zeolite addition and serves as a reference point to quantify the actual change in cell number over the incubation periods. The apparent decrease in T0 viability compared to untreated controls is an artifact of the MTT assay methodology: the zeolite particles present in the wells at T0 can interfere with formazan crystal formation or light absorbance measurement, resulting in slightly lower OD readings. This does not represent actual cell death but rather a measurement artifact at the initial time point.

2.10 Scratch wound assay

The scratch wound assay was used to see how zeolite affected the movement of L929 and HEK293T cells. Cells were seeded in 24-well plates at a density of 2×10^5 cells/well and cultured until reaching approximately 90–95% confluency. A scratch was then made with a 200 µL pipette tip to create a wound area between the cells. After that, the prepared zeolite doses were put into the wells. After that, pictures were taken at 0 h with an inverted microscope, and more pictures were taken after a 24-h incubation period. ImageJ Fiji software was used to measure the size of the wound area in each picture. Using the formula given by Liang et al. and statistical analysis, we found the migration area percentage for each dose [19]. It should be noted that mitomycin C was not used in this study; therefore, the observed wound closure reflects a combination of both cell migration and proliferation. The 24-h time point was selected based on established protocols in the literature [19] to minimize the confounding effect of cell proliferation on migration assessment, as extended time points would increase the contribution of proliferation to wound closure. %Migration Area = (%Migration Area at t0-%Migration Area at t24)/(%Migration Area at t0) × 100.

In this formula, t0 refers to the migration area percentage at 0 h, and t24 refers to the migration area percentage after 24 h of incubation [20].

2.11 Statistical analysis

The obtained data are presented as mean ± standard deviation (SD). Statistical analysis was performed using one-way analysis of variance (one-way ANOVA) followed by Dunnett's multiple comparison test against the control group. A p-value of < 0.05 was considered statistically significant. All results were visualized using GraphPad Prism (GraphPad Software, USA). For the MTT assay, each experiment was independently repeated three times with $n = 6$ wells per condition in each experiment (3 independent biological replicates × 6 technical replicates). For the scratch wound assay, $n = 3$ independent experiments were performed.

3 Results

3.1 XRD reflections specific to the crystalline phases of natural zeolite and purity assessment

We utilized Cu-Kα radiation (λ = 1.54060 Å) to find out the mineral composition and crystalline phase of the natural zeolite (Fig. 1). The diffractogram showed that there were characteristic zeolitic peaks, with clinoptilolite-series minerals being the most common phase. Semi-quantitative phase analysis revealed that clinoptilolite constitutes approximately 72.9% of the sample, existing in potassium (31.8%), calcium (22.2%), and sodium (18.9%) forms. Heulandite-Ca 20.8% and minor Stilbite-Ca 6.2% were also found. The lack of quartz or feldspar impurity peaks shows that the zeolite is very pure.The sharp, high-intensity reflections observed at ~ 2θ = 9.8° and 22.4° confirm a highly crystalline HEU (heulandite–clinoptilolite) framework.

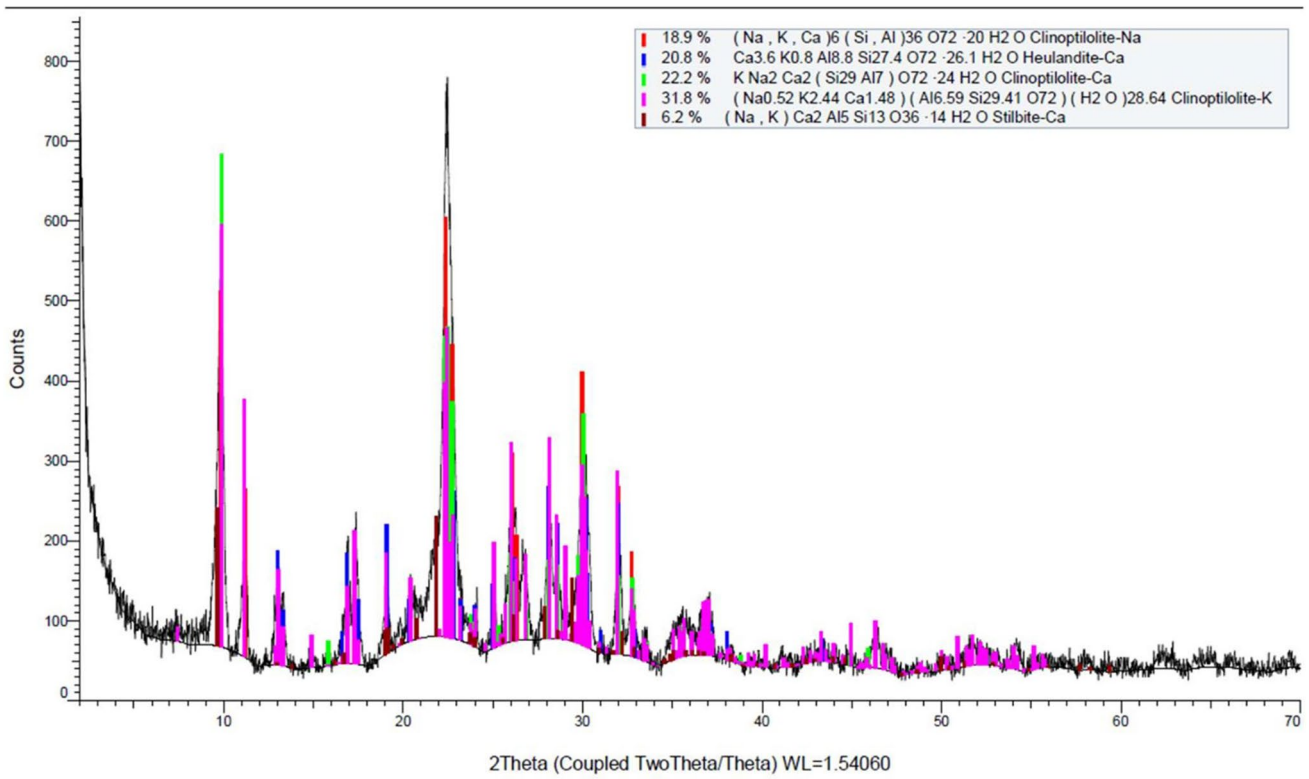

Fig. 1 XRD diffractogram of natural zeolite is shown. Colored bars indicate the different zeolitic phases identified (Clinoptilolite series, Heulandite and Stilbite) and their estimated weight percentages in the sample

3.2 XRF-based major oxide composition and Si/Al ratio evaluation of natural zeolite

The major oxide composition of the natural zeolite determined by XRF analysis is presented in Table 1. The XRF results show that the zeolite has a lot of silica. The SiO_2 content is between 61 and 71%, and the Al_2O_3 content is between 11.5% and 13.1%. The Si/Al ratio (4.8–5.4) is in the normal range for clinoptilolite-type zeolites. The sample also had CaO (2.7–5.2%), K_2O (2.2–3.4%), MgO (0.6–1.2%), and low levels of Fe_2O_3 (0.7–1.9%). These numbers show that the structure is mostly made up of Ca and K. The fact that it has a low Fe_2O_3 content also supports the mineralogical purity of the material.

Table 1 Major oxide composition of natural zeolite (wt%)

Major oxide	Content (%)
SiO_2	61–71%
Al_2O_3	11,5–13,1%
SiO_2/Al_2O_3	4,8–5,4%
Fe_2O_3	0,7–1,9%
MgO	0,6–1,2%
CaO	2,7–5,2%
Na_2O	0,2–13%
TiO_2	0,1–0,3%
K_2O	2,2–3,4%

Major oxide compositions are expressed in weight percentage (wt%), which is the standard convention in mineralogical and geochemical analyses (XRF results)

3.3 Trace element and heavy metal profile of natural zeolite

ICP-MS analysis demonstrated that the sample has a trace element profile that is similar to that of natural zeolitic formations. We looked at 47 elements in total, and their amounts are shown in Table 2. Lead (34 ppm), arsenic (16 ppm), cadmium (0.17 ppm), and chromium (3 ppm) were found in low amounts among the heavy metals. The sample contained rare earth elements (REEs) like Ce (44 ppm), La (19.5 ppm), Y (24.1 ppm), and Yb (2.6 ppm), which supports the idea that it came from tuff. The high levels of Ba (1205 ppm) and Sr (689 ppm) are also in line with the mineralogical traits of the area. The elemental profile shows that the sample is a geologically clean and high-purity zeolite.

3.4 Bulk density, pH, moisture, and macroscopic characteristics of natural zeolite

The natural zeolite's bulk density was found to be 0.431 g/cm^3, which means it has a low density and a lot of holes.

Table 2 Elemental composition and concentrations of natural zeolite

Ag: 0,42 ppm	Cr: 3 ppm	Lu: 0 ppm	S: < 0,01%	Ti: 0,05%
Al: 5,76%	Cs: 54 ppm	Mg:0,60%	Sb: 0,84 ppm	Tl: 1 ppm
As:16 ppm	Cu: 1,20 ppm	Mn:182 ppm	Sc: 3 ppm	U: 6,25 ppm
Ba: 1205 ppm	Fe:0,86%	Mo: 1 ppm	Se: < 3 ppm	V: 4 ppm
Be: 4 ppm	Ga: 13 ppm	Na: 0,25%	Sn: 3,9 ppm	W: < 1 ppm
Bi: 0 ppm	Hf: 3,17 ppm	Nb: 15,50 ppm	Sr: 689 ppm	Y: 24,1 ppm
Ca: 2,11%	In: 0,03 ppm	Ni: 6 ppm	Ta: 1,46 ppm	Yb: 2,6 ppm
Cd:0,17 ppm	K: 2%	P: 0,01%	Tb: 0,59 ppm	Zn: 30 ppm
Ce: 44 ppm	La:19,5 ppm	Pb: 34 ppm	Te: < 0,05 ppm	Zr: 74 ppm
Co: 0,80 ppm	Li:28 ppm	Rb: 122 ppm	Th: 30,20 ppm	

Trace element concentrations (ICP-MS results) are reported in ppm,following standard analytical conventions

Table 3 Physical properties of natural zeolite

BET surface area	49.0144 m^2/g
Single-Point Surface Area	48.4182 m^2/g
Average Pore Diameter (4 V/A by BET)	178.568 Å
Bulk Density	0.431 g/cm^3
pH	6.5–7.5
Moisture	5%
Appearance	87% white, 9.9% yellow
Odor	Odorless

The sample had a pH of 6.5 to 7.5, a moisture content of 5%, and a mostly white color (87%) with a few yellowish tones (9.9%).The material was odorless and displayed stable physical characteristics (Table 3).

3.5 Cation exchange capacity of the natural zeolite

Using the classical acetate exchange method with sodium acetate (NaOAc) and ammonium acetate (NH_4OAc) solutions, the total cation exchange capacity of the zeolite sample was determined as 2.38 meq/g (≈ 2.07 cmol/kg). This CEC value is consistent with the analytically measured exchangeable cation content of the material.

3.6 Morphological features and granulometric profile of natural zeolite

The surface morphology and particle size characteristics of natural zeolite were examined at 5,000 × magnification (Fig. 2). SEM images demonstrated that the particles exhibit irregular geometries, non-uniform shapes, and a rough surface topology. Particle size distribution appeared polydisperse. Spot measurements indicated that major particle clusters ranged between 7.07 µm and 10.06 µm. It was especially common to see finer particles, like agglomerated clusters, around the larger particles. These particles were less than 2 µm in size. The angular and locally platy crystal shape is what you would expect from natural zeolite. The pronounced surface roughness and agglomeration suggest that the surface area and porosity are higher, which may make the material better at adsorbing and catalyzing.

3.7 The effect of zeolite on L929 and HEK293T cell proliferation

Zeolite demonstrated a proliferation-enhancing effect on the L929 cell line with rising doses and extended incubation periods. After 24 h of incubation, doses of 500 and 600 µg/mL showed a statistically significant increase in proliferation compared to the control group (*$p < 0.05$, **$p < 0.01$) (Fig. 3.A). After 72 h of incubation, a dose of 500 µg/mL showed a highly significant proliferative effect (****$p < 0.0001$) (Fig. 3C).

Zeolite exhibited dose- and time-dependent proliferation-enhancing effects on the HEK293T cell line at each incubation period. At the end of the 24 h incubation, significant proliferative effects were observed at 400, 500, and 600 µg/mL (*$p < 0.05$, ****$p < 0.0001$) (Fig. 4.A); at the end of the 48 h incubation, at 300, 400, 500, and 600 µg/mL (**$p < 0.01$, ***$p < 0.001$, ****$p < 0.0001$) (Fig. 4.B); and at the end of the 72 h incubation, 600 µg/mL showed a statistically significant proliferative effect compared to the control group (Fig. 4.C) (****$p < 0.0001$).

3.8 The effect of zeolite on L929 and HEK293T cell migration

The effects of zeolite on L929 cell migration after 24 h are shown (Fig. 5.A). According to the statistical analysis, the increase in L929 cell migration at 24 h was significant at the 200 µg/mL zeolite dose (**$p < 0.01$) (Fig. 5.B).

The effects of zeolite on HEK293T cell migration after 24-h are shown (Fig. 6.A). According to the statistical analysis, the increase in HEK293T cell migration after 24 h was significant at a zeolite dose of 100 µg/mL (***$p < 0.001$) (Fig. 6.B). Moreover, the inhibitory effects of higher zeolite doses on cell migration were significant at 400 and 500 µg/mL (**$p < 0.01$, *$p < 0.05$).

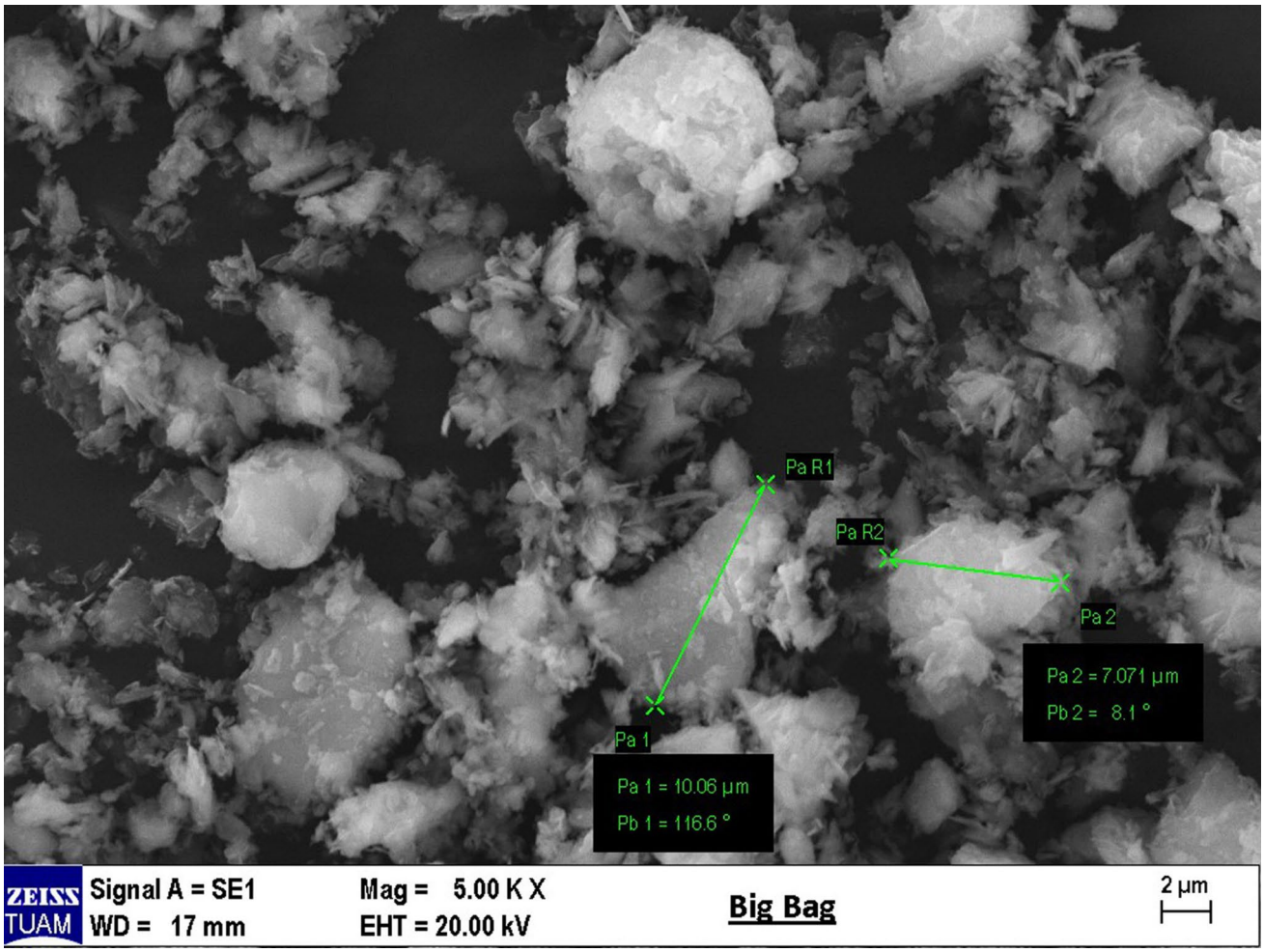

Fig. 2 SEM micrograph of the natural zeolite sample (5.00 K × magnification, 20.000 kV). The image shows particles with irregular morphology and typical particle sizes in the 7–10 µm range

4 Discussion

It is known that the purity of natural clinoptilolite varies over a considerably wide range in the literature [21]. In our study, the XRD analysis of natural zeolite (Fig. 1.) shows that the dominant phase of the sample consists of clinoptilolite series minerals at an approximate ratio of 72.9%, indicating that it is a high-purity natural zeolite. Furthermore, Heulandite-Ca 20.8% and minor Stilbite-Ca 6.2% phases were also detected. The purity of natural clinoptilolite samples is reported to vary between 50 and 90% in the literature [22]. The 72.9% clinoptilolite ratio in our study is consistent with the high-purity range reported in the literature. Akyalcin et al. [23]. Draw attention to the presence of sharp reflections specific to the HEU framework, which confirms the crystalline structure of natural zeolite. The sharp and high-intensity reflections we found at ~ $2\theta = 9.8°$ and 22.4° support this high crystallinity and the presence of the HEU framework [23, 24].

According to the XRF results (Table 1), the Si/Al ratio of the sample was determined to be 4.8–5.4%. It is stated in the literature that the Si/Al ratio of clinoptilolites typically ranges between 4.0% and 5.5% [21]. In our study, our Si/Al ratio is close to the upper limit of this range, which confirms the high silica content 61–71% associated with a more hydrophobic surface and higher acid resistance [13, 25]. In the analysis conducted by Sprynskyy et al., the Al_2O_3 content of the clinoptilolite sample was determined as 11.5%, which is consistent with the typical clinoptilolite values of 11.5–13.1% determined in our study [26]. Calvo et al. reported that the Fe_2O_3 value in a natural zeolite sample analyzed was around 5.25% [27]. The Fe_2O_3 value of the sample in our study is 0.7–1.9%, confirming a low level of impurity and supporting its biocompatibility potential [21].

The CP-MS analysis (Table 2) shows trace element profiles that show where the sample came from geographically. The high levels of cations, especially Ba 1205 ppm and Sr 689 ppm, fit with the minerals that are common in the area.

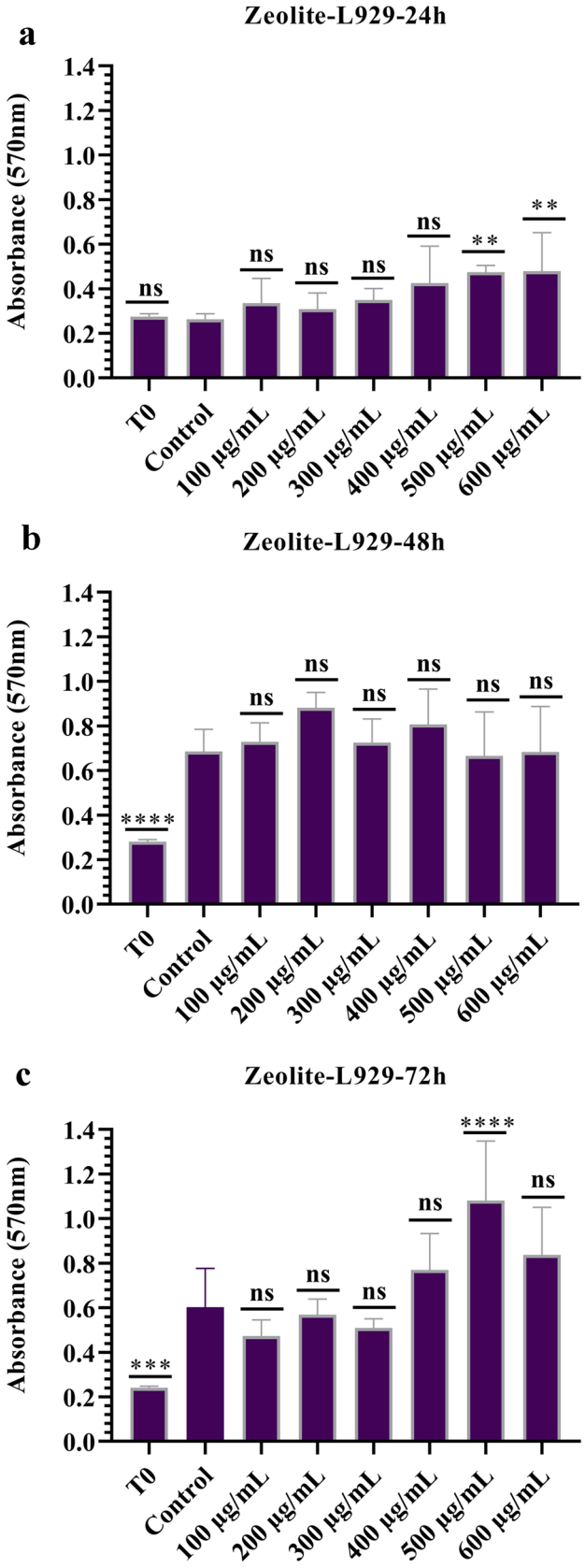

Fig. 3 Effects of different zeolite doses on L929 cell proliferation. Cell proliferation following **a** 24, **b** 48, and **c** 72 h of incubation is shown. Data are presented as mean ± standard deviation (SD), $n = 6$. Statistical analysis was performed using one-way ANOVA followed by Dunnett's multiple comparison test versus the control group (T0: Time zero). (ns: $p > 0.05$, *$p < 0.05$, **$p < 0.01$, **** $p < 0.0001$; compared to the control group.)

The low levels of heavy metals detected, Pb 34 ppm, As 16 ppm, Cd 0.17 ppm are an important biological safety parameter indicating the material's suitability for use in health applications [28]. At the highest tested dose (600 µg/mL), the calculated Pb exposure would be approximately 0.02 µg/mL, which is well below the cytotoxic thresholds reported in the literature for cell culture applications [29]. Similarly, the effective As [30] and Cd [31] concentrations at this dose would be approximately 0.0096 µg/mL and 0.0001 µg/mL, respectively, both substantially below levels associated with cellular toxicity. In our study, the CEC value of natural zeolite was determined as 2.38 meq/g (≈ 2.07 cmol/kg). Tsvetanova et al. stated that the CEC values of clinoptilolites typically range between 1.5 and 2.5 meq/g [32]. The value obtained in our study is close to the upper limit of this range, indicating high ion-exchange capacity and thus the suitability of the zeolite for functionalization with metal ions or adsorption applications [32, 33]. Furthermore, the BET surface area 49.0144 m^2/g and bulk density 0.431 g/cm^3 of natural zeolite (Table 3) in our study indicate a low-density and highly porous structure. Akyalcin et al. highlighted that natural zeolites typically exhibit low density and large pore volume [23].

When the SEM analysis (Fig. 2) and particle morphology of natural zeolite in our study were evaluated, the particles were found to have irregular, clustered geometries, with sizes mostly ranging from 7.07 to10.06 µm. Fine particles under 2 µm were also detected around larger clusters. A study by Wang et al. suggested that a zeolite particle size between 1 – 10 µm in tissue regeneration applications is optimized for cell interaction and biological activity due to a better surface area-to-volume ratio [29]. The 7–10 µm range and the presence of fine particles in our findings indicate that the material has a suitable morphology for cell-level interaction [29, 34].

When considered together, the physicochemical properties of this natural zeolite can be directly correlated with its observed biological effects. The high Si/Al ratio (4.8–5.4) confers greater surface hydrophobicity and acid resistance, which may enhance the material's stability in the cell culture environment and sustain its bioactivity over extended incubation periods. The high CEC value (2.38 meq/g) enables controlled release of bioavailable cations such as Ca^{2+} and Mg^{2+}, which are known to promote cell adhesion,

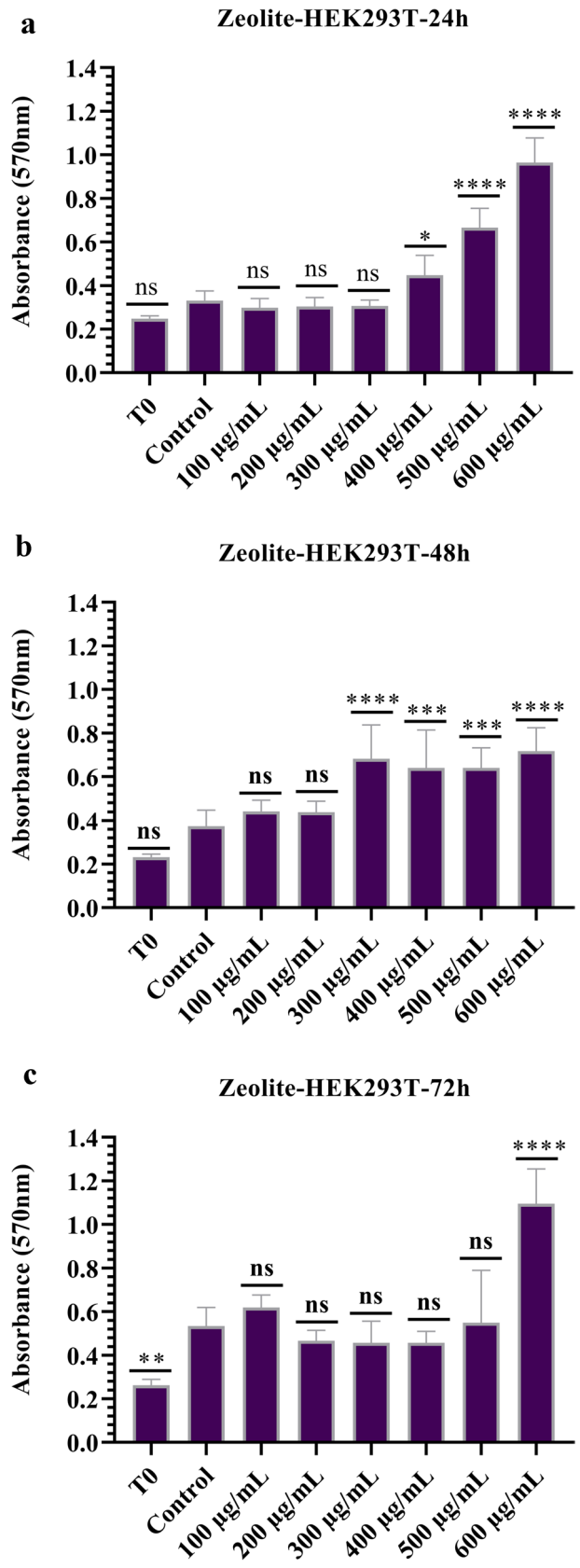

Fig. 4 Effects of different zeolite doses on HEK293T cell proliferation. Cell proliferation following **a** 24, **b** 48, and **c** 72 h of incubation is shown. Data are presented as mean ± standard deviation (SD), $n = 6$. Statistical analysis was performed using one-way ANOVA followed by Dunnett's multiple comparison test versus the control group (T0: Time zero). (ns: $p > 0.05$, *$p < 0.05$, **$p < 0.01$, *** $p < 0.001$, **** $p < 0.0001$; compared to the control group.)

proliferation, and migration through integrin-mediated signaling pathways. Furthermore, the BET surface area (49.01 $m.^2/g$) combined with the 7–10 µm particle size provides an optimal surface area-to-volume ratio for efficient cell–material interaction, supporting the dose-dependent proliferative effects observed in both L929 and HEK293T cells [15, 16, 22, 33, 34].

In our study, the zeolite was incubated with the L929 fibroblast cell line at different concentrations (100, 200, 300, 400, 500 and 600 µg/mL) and its effects on cell viability were evaluated by MTT assay after 24, 48, and 72 h of incubation (Fig. 3.). The effect of zeolite on cell viability was observed to increase with increasing dose and prolonged incubation time. According to the literature, zeolite is reported to be non-toxic and to increase cell proliferation in fibroblast cell lines such as HDF, IMR-90, 3T3, and NIH/3T3 [8, 9, 15, 16]. These findings support our results, which show that zeolite increases proliferation in the L929 cell line. The relatively higher standard deviations observed at 400 and 600 µg/mL (Fig. 3A) may be attributed to increased particle-related interference with absorbance readings at higher zeolite concentrations. Additionally, the non-linear temporal response observed at 500 µg/mL with a relative decrease at 48 h followed by a significant increase at 72 h (Fig. 3B, C) may reflect an initial transient adaptive response of cells to the zeolite particles, such as temporary cell cycle arrest or metabolic adjustment, followed by a subsequent robust proliferative response.

Zeolite also increased proliferation in HEK293T epithelial cells in parallel with increasing doses (100, 200, 300, 400, 500 and 600 µg/mL) and incubation times (24, 48, and 72 h) (Fig. 4.). No study was found in the literature examining the effects of natural zeolite on HEK293T kidney epithelial cells. However, synthetic molecules containing zeolite have been shown to increase proliferation in epithelial cells, including human embryonic kidney cells (HEK293), without causing cytotoxic effects. This fact supports the proliferative effect observed in our study [13]. While a formal IC50 determination was not performed, as the focus of our study was to identify the proliferative concentration range rather than cytotoxic thresholds, we acknowledge this as a limitation. Formal IC50 determination should be conducted in future studies to establish a complete safety profile of natural zeolite for biomedical applications.

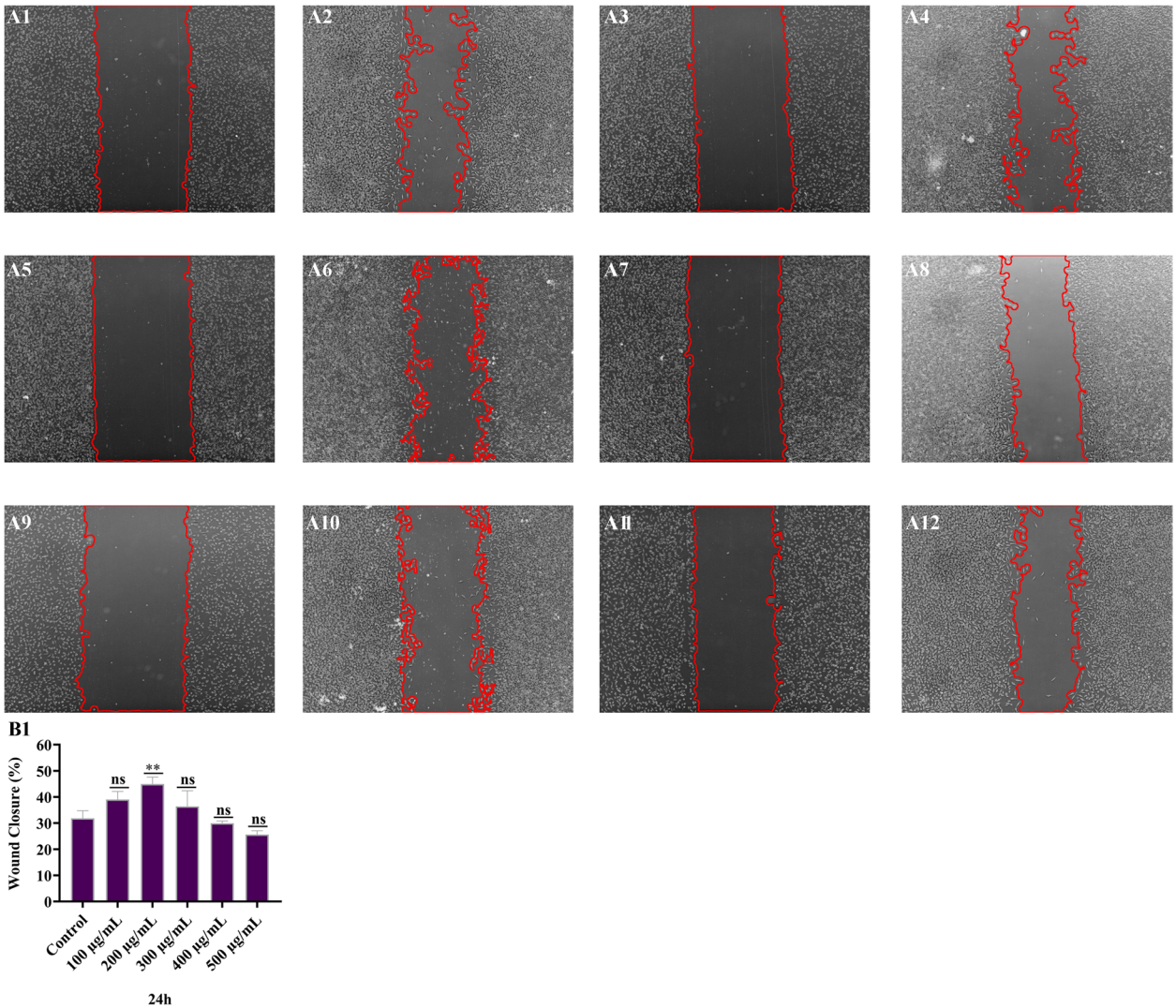

Fig. 5 The effect of zeolite on migration in the L929 cell line is shown. **a** Migration images of cells treated with zeolite doses at 0 and 24 h are presented. **b** The percentage of the closed area after migration is given. Data are presented as mean ± standard deviation (SD), $n = 3$. Statistical analysis was performed using one-way ANOVA followed by Dunnett's multiple comparison test versus the control group (ns: $p > 0.05$, $^{**}p < 0.01$; compared to the control group)

In our study, the effects of zeolite on cell migration were evaluated by the wound healing test. Following 24 h of incubation with zeolite (100, 200, 300, 400 and 500 µg/mL) L929 cell migration was observed to increase, but only the 200, µg/mL dose provided a statistically significant increase compared to the control group ($^{**}p < 0.01$) (Fig. 5.B.). Similarly, zeolite increased HEK293T cell migration at low doses (100, 200, and 300 µg/mL); however, only the 100 µg/mL dose showed a significant difference compared to the control group ($^{***}p < 0.001$) (Fig. 6.B.). These findings are consistent with the current literature. For example, Kocaaga et al. showed that synthetic molecules containing zeolite increased the migration of PCS-201–012 human dermal fibroblasts [12]. Similarly, Zheng et al. reported that synthetic molecules containing zeolite increased proliferation and migration in both L929 fibroblasts and HaCaT keratinocyte-derived epithelial cells [35].

The design is important to consider the dose-dependent effects of natural zeolite on cell migration, particularly the biphasic response observed in HEK293T cells, which is marked by stimulation at low concentrations (100–200 µg/mL) and inhibition at elevated doses (400–500 µg/mL). There are many reasons why biphasic phenomena happen, and they are often seen when particles and cells interact. Clinoptilolite may help control the release of beneficial trace elements (like Ca^{2+} and Mg^{2+}) or adsorb inhibitory factors from the culture medium at lower concentrations because it has a large surface area and can exchange ions. This might make a small area that makes cells move. On the other hand, when there are too many particles, they

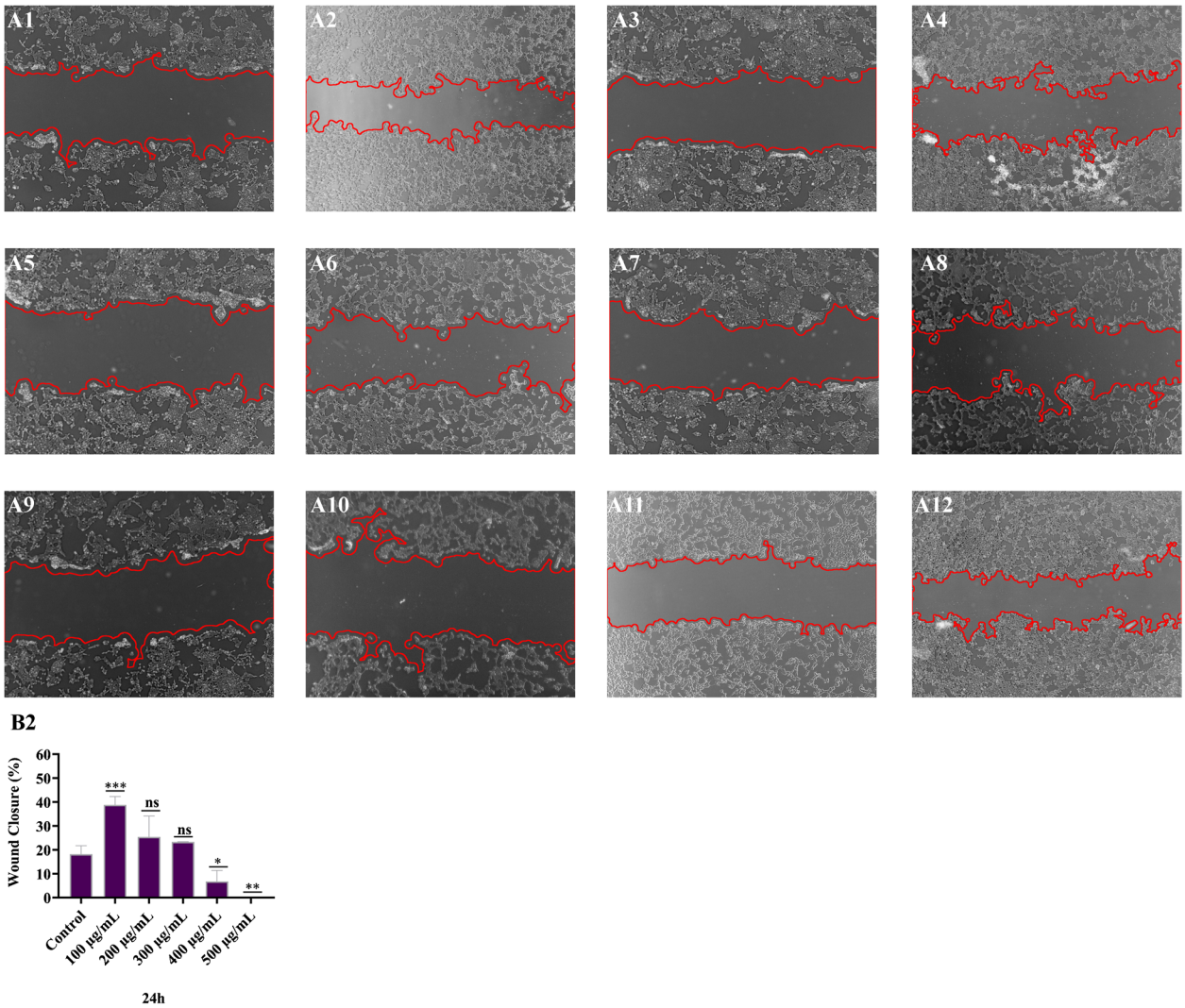

Fig. 6 The effect of zeolite on migration in the HEK293T cell line is shown. **a** Migration images of cells treated with zeolite doses at 0 and 24 h are presented. **b** The percentage of the closed area after migration is given. Data are presented as mean ± standard deviation (SD), $n = 3$. Statistical analysis was performed using one-way ANOVA followed by Dunnett's multiple comparison test versus the control group (ns: $p > 0.05$, *$p < 0.05$, **$p < 0.01$, ***$p < 0.001$; compared to the control group)

can settle out and make it harder for cells to move, break down cell adhesion structures, or cause mild cellular stress that makes cells work less well for a short time. On the other hand, too many particles at higher concentrations can cause sedimentation that makes it harder for cells to move, breaks up cell adhesion structures, or causes mild cellular stress that makes cells work less well without killing them. Moreover, the aggregation of zeolite particles observed in our SEM analysis at elevated concentrations may have reduced the material's bioavailability or created a physical barrier that obstructed cellular movement. This biphasic dose–response pattern is consistent with the literature on particle-cell interactions. Calabrese [36] demonstrated that biphasic dose–response characteristics are a common phenomenon in cell migration, independent of the target tissue and chemoattractant agent. Furthermore, at higher particle concentrations, gravitational sedimentation increases the effective dose delivered to adherent cells, as demonstrated by in vitro sedimentation-diffusion-dosimetry models, which may amplify the inhibitory effects observed at elevated zeolite concentrations. Additionally, Zarrintaj et al. [34] reported that zeolite ion release follows concentration-dependent kinetics that can shift from stimulatory to inhibitory ranges, supporting the biphasic response observed in our study. Future studies should include ion release profiling at different zeolite concentrations and particle sedimentation analysis to further elucidate this phenomenon. It should also be noted that mitomycin C was not used in the scratch wound assay; therefore, the observed wound closure reflects a combination of both cell migration and proliferation. At

the 24-h time point, the contribution of proliferation is expected to be relatively modest compared to migration, particularly for the L929 fibroblast cells. Nevertheless, future studies should incorporate anti-proliferative agents such as mitomycin C to isolate the migratory component and provide a more precise assessment of zeolite's effect on cell migration. Although complete wound closure was not observed at 24 h for all treatment groups, extending the evaluation to later time points (48, 72 h) would increase the contribution of cell proliferation, complicating the interpretation of migration-specific effects. Future studies using time-lapse imaging combined with anti-proliferative agents at multiple time points (24, 48, 72 h) would provide a more comprehensive and accurate assessment of zeolite's effect on cell migration kinetics. Our findings clearly show that natural zeolite has the ability to promote migration and proliferation, but we still don't know exactly how these effects work at the molecular level. This is a big problem with the current study, which was meant to be a first step in figuring out the biological properties of the material.

Even though we didn't look into any particular signaling pathways, the literature currently in publication offers tenable mechanistic theories that could be explored further. For example, Keeting et al. [37] showed that zeolites may alter the secretion of autocrine or paracrine growth factors by increasing the production of transforming growth factor-beta (TGF-β) in osteoblast-like cells. According to a more recent study by Qi et al. [38], cerium-doped zeolite nanoparticles improve the migration and proliferation of endothelial cells by controlling the PI3K and VEGF/VEGFR2 signaling axes. Similar pathways may be involved in the responses seen in our L929 and HEK293T models, since TGF-β and VEGF are also important regulators of fibroblast and epithelial cell function during wound healing. To identify the ways in which natural clinoptilolite influences cell behavior in a positive way, future research should use targeted molecular techniques, such as Western blot analysis of important signaling nodes (PI3K/Akt, MAPK/ERK, etc.) and growth factor expression measurement.When all the results of our study are evaluated, the natural zeolite has physicochemical properties such as high-purity clinoptilolite content (72.9%), high Si/Al ratio (4.8—5.4%), and high CEC capacity 2.38 meq/g (≈ 2.07 cmol/kg). Having an appropriate particle size 7.07—10.06 µm morphologically, it shows that natural zeolite carries high potential for biomedical applications. Our in vitro findings show that natural zeolite significantly supports proliferation and increases cell migration at low/medium doses in L929 fibroblast and HEK293T epithelial cell lines with increasing dose and incubation times. This suggests that natural zeolite may be a suitable candidate for further investigation for fibroblast proliferation and epithelialization, which are the fundamental processes of periodontal wound healing, especially in biomedical applications.

It is important to emphasize that the novelty of the present study lies in its comprehensive, multi-technique physicochemical characterization of a natural, unmodified clinoptilolite-type zeolite combined with systematic dose–response and time-course biological screening across two distinct cell types. While previous studies have primarily focused on synthetic or chemically modified zeolites (e.g., metal-ion loaded, nanoparticle-doped, or composite scaffolds), the present work provides essential baseline data on the inherent biological activity of the unprocessed material. This combined characterization–biology approach, rarely reported in a single study, offers a unique contribution to the field and lays the groundwork for future rational functionalization strategies.

A significant limitation of the current study is the lack of mechanistic data that clarifies the molecular pathways by which natural zeolite induces its pro-proliferative and pro-migratory effects. Although our results unequivocally illustrate the biological activity of this clinoptilolite-rich material, the fundamental mechanisms have yet to be elucidated. According to the literature, there are a number of reasonable hypotheses that need to be looked into. Zeolites are known to change the ionic microenvironment in the area around them because they can exchange a lot of cations. This could release bioavailable ions (like Ca^{2+} and Si^{4+}) that influence cell adhesion, proliferation, and migration [16]. Zeolites can also absorb and concentrate growth factors or extracellular matrix proteins from the culture medium, which can improve integrin-mediated signaling and cell–matrix interactions [8, 17]. Keeting et al. [36] specifically showed that zeolite A increases the production of transforming growth factor-beta (TGF-β) in osteoblast-like cells. This suggests that it may work through an autocrine or paracrine mechanism. Since TGF-β is a key regulator of fibroblast and epithelial cell function in wound healing, this pathway is a promising target for future research. To this end, future mechanistic investigations should include the following: (1) reactive oxygen species (ROS) measurement using the DCFH-DA assay to assess oxidative stress responses; (2) apoptosis and necrosis assessment via Annexin V/PI staining and flow cytometry; (3) Western blot analysis of critical signaling nodes including phosphorylated PI3K/Akt, MAPK/ERK1/2, and Smad2/3; (4) quantitative PCR for evaluating the expression of key growth factors such as TGF-β, VEGF, and FGF; and (5) use of specific pathway inhibitors (e.g., LY294002 for PI3K, U0126 for MEK/ERK, and SB431542 for TGF-β receptor) to elucidate the exact signaling mechanisms through which natural clinoptilolite modulates cellular behavior.

Another important thing to think about is how well the epithelial cell model used can be used in translation. HEK293T cells are a significant and extensively employed resource for examining essential elements of human epithelial cell biology [13], they do not accurately reflect the oral epithelium. The complex and differentiated phenotype of gingival keratinocytes markedly contrasts with that of embryonic kidney epithelial cells. Consequently, the identified pro-migratory and pro-proliferative effects on HEK293T cells cannot be directly applied to oral epithelial wound healing without additional confirmation. Therefore, validation of the present findings using primary human gingival fibroblasts, immortalized oral keratinocyte cell lines (e.g., OKF6/TERT-2, HOK), or three-dimensional oral tissue models is essential to confirm the translational relevance of the observed biological effects to periodontal wound healing.

To address these constraints, subsequent research should employ targeted molecular methodologies, including Western blot analysis of critical signaling nodes (e.g., phosphorylated ERK1/2, Smad2/3), quantitative PCR for assessing the expression of TGF-β and other growth factors, and specific pathway inhibitors to elucidate the exact mechanisms through which natural clinoptilolite enhances cellular responses. To validate the applicability of our findings to periodontal tissue regeneration, these mechanistic investigations should be conducted in more clinically pertinent models, such as primary human gingival fibroblasts, oral keratinocytes (e.g., HaCaT), or immortalized oral epithelial cell lines (e.g., OKF6/TERT-2). Additionally, future studies should evaluate the antibacterial effects of natural zeolite against common periodontal pathogens, including *Porphyromonas gingivalis*, *Aggregatibacter actinomycetemcomitans*, and *Fusobacterium nucleatum*, to provide a comprehensive assessment of the material's potential for periodontal applications. Besides making this material more useful for real-world applications, this kind of research would also help make zeolite-based formulations that are perfect for biomedical use.

5 Conclusion

The current study offers initial in vitro evidence indicating that natural clinoptilolite-type zeolite is biocompatible and induces positive cellular responses in fibroblast and epithelial cell models. These preliminary results suggest that natural zeolite merits further investigation as a potential candidate for periodontal tissue engineering and wound healing applications. However, it must be emphasized that the extrapolation of these in vitro findings to clinical significance requires extensive validation, including in vivo studies to assess tissue-level responses, mechanistic investigations to elucidate the molecular pathways underlying the observed effects, evaluation in clinically relevant cell models such as primary human gingival fibroblasts and oral keratinocytes, and assessment of hemostatic and antibacterial characteristics. Future studies incorporating targeted molecular assays and more physiologically relevant models are essential before any clinical translation can be considered.

Supplementary Information The online version contains supplementary material available at https://doi.org/10.1007/s10934-026-01925-y.

Author contributions N.A.K. and H.H.E contributed to the conceptualization, study design, and manuscript drafting. All authors contributed to data acquisition. N.A.K. and B. I. supervised the study. A.Y.C project administration. All authors reviewed and approved the final version of the manuscript.

Funding Open access funding provided by the Scientific and Technological Research Council of Türkiye (TÜBİTAK). This research received no external funding.

Data availability No datasets were generated or analysed during the current study.

Declarations

Competing interest The authors declare no competing interests.

Open Access This article is licensed under a Creative Commons Attribution 4.0 International License, which permits use, sharing, adaptation, distribution and reproduction in any medium or format, as long as you give appropriate credit to the original author(s) and the source, provide a link to the Creative Commons licence, and indicate if changes were made. The images or other third party material in this article are included in the article's Creative Commons licence, unless indicated otherwise in a credit line to the material. If material is not included in the article's Creative Commons licence and your intended use is not permitted by statutory regulation or exceeds the permitted use, you will need to obtain permission directly from the copyright holder. To view a copy of this licence, visit http://creativecommons.org/licenses/by/4.0/.

References

1. Y.D. Cho, K.H. Kim, Y.M. Lee, Y. Ku, Y.J. Seol, Pharmaceuticals **14**, 456 (2021). https://doi.org/10.3390/ph14050456
2. L.J. Li, C.H. Chu, O.Y. Yu, Nanomaterials **13**, 2973 (2023). https://doi.org/10.3390/nano13222973
3. I. Siora, L. Andriyko, I. Gerashchenko, M. Borysenko, E. Pakhlov, O. Oranska, Microporous Mesoporous Mater. **397**, 113778 (2025)
4. T. Pandya, S. Patel, M. Kulkarni, Y.R. Singh, A. Khodakiya, S. Bhattacharya, B.P. Prajapati, Heliyon **10**, e36417 (2024)
5. S. Deshpande, S. Kheur, M. Kheur, T.F. Eyüboğlu, M. Özcan, Curr. Oral Health Rep. **10**, 36 (2023)
6. G.M.M. Demiti, N.C. Homem, H.P. Felgueiras, A.C. Ribeiro, B.A.A. Filho, M.H.N.O. Scaliante, Microporous Mesoporous Mater. **396**, 113689 (2025)

7. F. Morante-Carballo, N. Montalván-Burbano, P. Carrión-Mero, K. Jácome-Francis, Sustainability **13**, 6378 (2021)
8. N. Ninan, M. Muthiah, N.A. Yahaya, I.K. Park, A. Elain, T.W. Wong, Colloids Surf. B Biointerfaces **115**, 244 (2014)
9. M. Neidrauer, U.K. Ercan, A. Bhattacharyya, J. Samuels, J. Sedlak, R. Trikha, J. Med. Microbiol. **63**, 203 (2014)
10. S. Mohandesnezhad, Y. Pilehvar-Soltanahmadi, E. Alizadeh, A. Goodarzi, S. Davaran, M. Khatamian, Mater. Chem. Phys. **252**, 123152 (2020)
11. M.A.F. Maghsoudi, R.A. Asbagh, S.M.A. Tafti, R.M. Aghdam, A. Najjari, P.S. Pirayvatlou, L. Foroutani, A.R. Fazeli, Int. J. Biol. Macromol. **295**, 139348 (2025)
12. B. Kocaaga, O. Kurkcuoglu, M. Tatlier, G. Dinler-Doganay, S. Batirel, F.S. Güner, Polymers **14**, 460 (2022)
13. H. Jahangirian, R. Rafiee-Moghaddam, N. Jahangirian, B. Nikpey, S. Jahangirian, N. Bassous, Int. J. Nanomedicine **15**, 1005 (2020)
14. K. Yomthong, J. Phys. Chem. C (in press) (2024)
15. I. Biblioteca, M. Sambucci, M. Valente, Ceram. Int. **49**, 39649 (2023)
16. M. Fayezi, Z. Shiri-Yekta, H. Sepehrian, M. Heydari, M. Rahghoshay, S. Zolghadri, Sci. Rep. **13**, 19087 (2023). https://doi.org/10.1038/s41598-023-46285-4
17. D. Novembre, D. Gimeno, M. Calista, V. Mancinelli, E. Miccadei, Sci. Rep. **12**, 9284 (2022). https://doi.org/10.1038/s41598-022-13243-7
18. W. Legese, A.M. Taddesse, K. Kibret, L. Wogi, Heliyon **10**, e25524 (2024)
19. C.C. Liang, A.Y. Park, J.L. Guan, Nat. Protoc. **2**, 329 (2007)
20. A. Suarez-Arnedo, F.T. Figueroa, C. Clavijo, P. Arbeláez, J.C. Cruz, C. Muñoz-Camargo, PLoS ONE **15**, e0232565 (2020)
21. M. Senila, O. Cadar, Heliyon **10**, e25303 (2024)
22. N. Grasi, B. Ziantoni, D. Fino, M. Piumetti, Environ. Sci. Pollut. Res. 1 (2024)
23. S. Akyalcin, L. Akyalcin, E. Ertugrul, Res. Chem. Intermed. **50**, 1455 (2024)
24. F.S. Wanyonyi, F. Orata, G.K. Mutua, M.O. Odey, S. Zamisa, S.E. Ogbodo, F. Maingi, A. Pembere, Heliyon **10**, 34657 (2024)
25. N.S. Dionisiou, T. Matsi, in Environmental Materials and Waste, edited by M.N.V. Prasad and K. Shih (Academic Press, 2016), pp. 591–606
26. M. Sprynskyy, R. Golembiewski, G. Trykowski, B. Buszewski, J. Phys. Chem. Solids **71**, 1269 (2010)
27. B. Calvo, L. Canoira, F. Morante, J.M. Martínez-Bedia, C. Vinagre, J.E. García-González, J.R.A. Elsen, J. Hazard. Mater. **166**, 619 (2009)
28. S.K. Pavelić, J.S. Medica, D. Gumbarević, A. Filošević, N. Pržulj, K. Pavelić, Front. Pharmacol. **9**, 409213 (2018)
29. S. Wang, R. Li, D. Li, Z.Y. Zhang, G. Liu, H. Liang, Y. Qin, J. Yu, Y. Li, J. Mater. Chem. B **6**, 3254 (2018)
30. H. Wang, H. Wang, J. Guan, W. Guan, Z. Liu, Sci. Rep. **13**, 9670 (2023)
31. A. Al-Ghafari, E. Elmorsy, E. Fikry, M. Alrowaili, W.C. Carter, PLoS One **14**, e0225341 (2019)
32. L. Tsvetanova, B. Barbov, R. Rusew, Water **14**, 2152 (2022). https://doi.org/10.3390/w14142152
33. I. Rodríguez-Iznaga, M.G. Shelyapina, V. Petranovskii, Minerals **12**, 1628 (2022)
34. P. Zarrintaj, G. Mahmodi, S. Manouchehri, A.H. Mashhadzadeh, M. Khodadadi, M. Servatan, MedComm **1**, 5 (2020)
35. L. Zheng, X. Li, C. Xu, Y. Xu, Y. Zeng, M. Tam, H.T. Zhang, X. Wang, Adv. Healthc. Mater. **12**, 2300075 (2023)
36. P.E. Keeting, M.J. Oursler, K.E. Wiegand, S.K. Bonde, T.C. Spelsberg, B.L. Riggs, J. Bone Miner. Res. **7**, 1281 (1992)
37. Y. Qi, K. Qian, J. Chen, Y.E. E, Y. Shi, H. Li, L. Zhao, J. Nanobiotechnology 19, 414 (2021). https://doi.org/10.1186/s12951-021-00956-2
38. E.J. Calabrese, Crit. Rev. Toxicol. **31**, 615 (2001)

Publisher's Note Springer Nature remains neutral with regard to jurisdictional claims in published maps and institutional affiliations.